Supporting Information

Nano-Whiskers of Fe_2O_3 Coated with NiCo LDH Grown on Iron Foam Substrate for Large-Current Overall Water Splitting

Authors: Samina Hameed [1], Xiaolong Liang [1] Yousaf Khan [2], Ihtesham Ul Haq [3], Xueliang Mu**[4] and Jinxuan Liu*[1,4]

[1] *State Key Laboratory of Fine Chemicals, Dalian University of Technology, 116024 Dalian, China.*

[2]*Dalian Institute of Chemical Physics, Chinese Academy of Sciences, Dalian, Liaoning 116023, PR China*

[3]*State Key Laboratory of Structure Analysis, Optimization and CAE software for Industrial Equipment, Department of Engineering Mechanics, Dalian University of Technology, Dalian 116024, China*

[4] *Leicester International Institute, Dalian University of Technology, 124010 Panjin, China*

* *Jinxuan Liu - State Key Laboratory of Fine Chemicals, Dalian University of Technology, 116024 Dalian, China;Leicester International Institute, Dalian University of Technology, 124010 Panjin, China.*

***Xueliang Mu - Leicester International Institute, Dalian University of Technology, 124010 Panjin, China.*

* *Corresponding author.*

** *Corresponding author.*

E-mail address: jinxuan.liu@dlut.edu.cn (J. Liu); xueliang.mu@dlut.edu.cn (X. Mu)

All the potentials reported hereinafter were converted to reversible hydrogen electrode (RHE) using the Eq. (1):

$$E_{(RHE)} = E_{(Hg/HgO)} + 0.098 + 0.059 \times pH \qquad (1)$$

where $E_{(RHE)}$ is WE potential referred to RHE; $E_{(Hg/HgO)}$ and is the measured potential with Hg/HgO RE.

Cyclic voltammetry (CV) was performed in non-Faradaic potential window (-0.05 ~ 0.05 V vs. RHE) at different scan rates (20 ~ 140 mV s^{-1}) to evaluate the double layer capacitance (C_{dl}) of the catalytic materials, which is proportional to their electrochemically active surface area (ECSA). The ECSA was calculated according to the Eq. (2):

$$ECSA\cdot = \frac{C_{dl}}{C_s} \qquad (2)$$

Where C_{dl} was determined by the half the slope of the current density difference ($\Delta J = j_a - j_c$) at 1.04 V vs. scan rate plot; C_S is the specific capacitance of the material, which is 40 μF cm^{-2} based on typical reported values. [25]

The HER and OER linear sweep voltammetry (LSV) polarization curves were tested at a scan rate of 5 mV s^{-1} with iR-compensation. The corresponding Tafel plots and slopes were calculated according to the Eq. (3):

$$\eta = b \cdot \log j + C \qquad (3)$$

Where η, j, b, and C represent overpotential, current density, Tafel slope, and intercept, respectively.

The overpotentials of HER and OER were calculated according to Eq. (4) and Eq. (5), respectively:

$$\eta_{HER} = 0 - E_{(RHE)} \qquad (4)$$

$$\eta_{OER} = E_{(RHE)} - 1.23 \qquad (5)$$

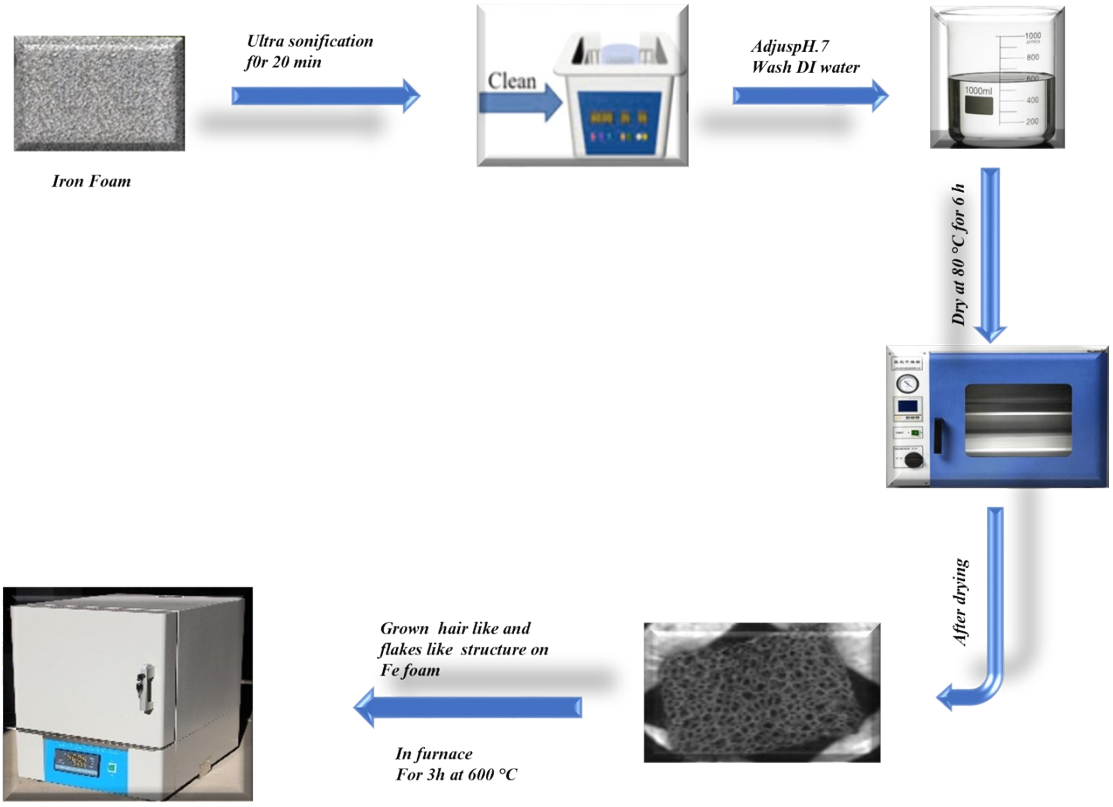

Fig. S1. Schematic illustration of the synthesis process for Fe_2O_3/Fe.

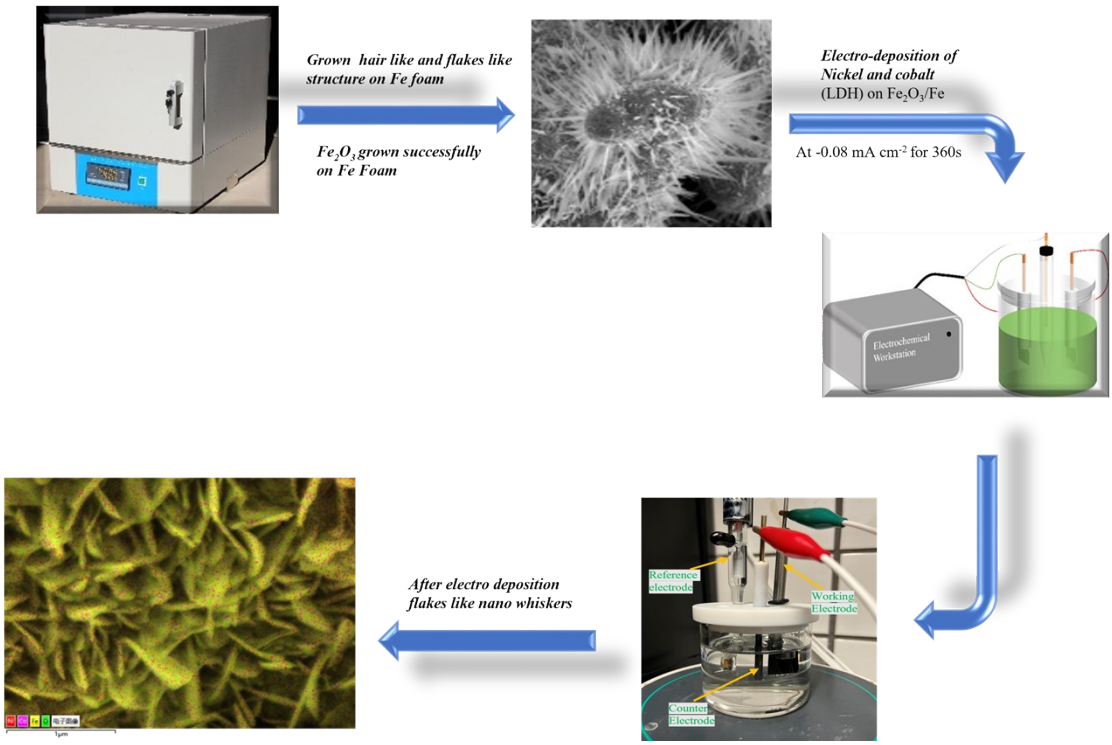

Fig. S2. Schematic illustration of the synthesis process for NiCo LDH/Fe.

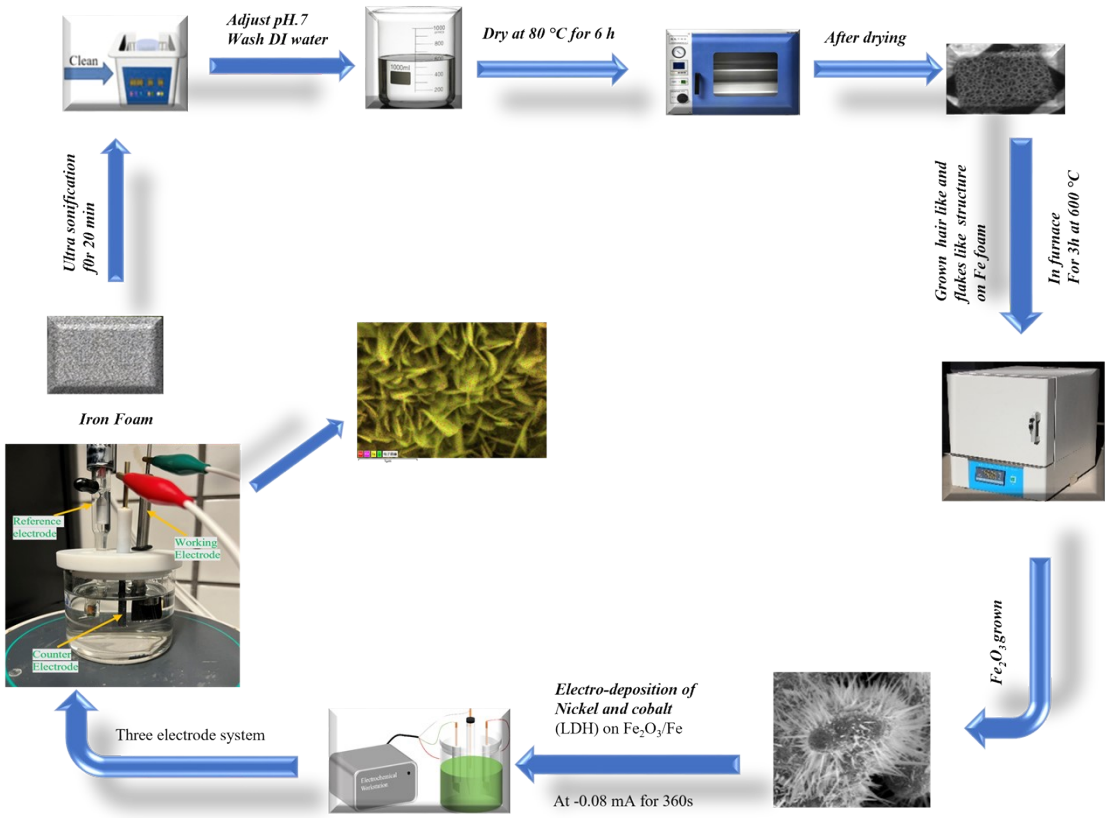

Fig. S3. Schematic illustration of the synthesis process for (NiCo LDH@Fe_2O_3)/Fe.

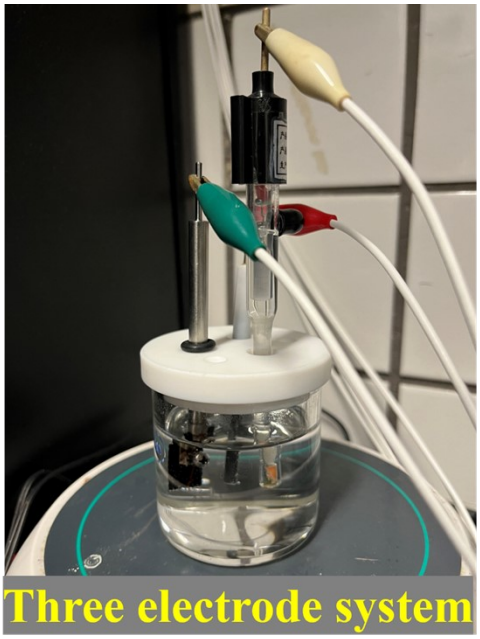

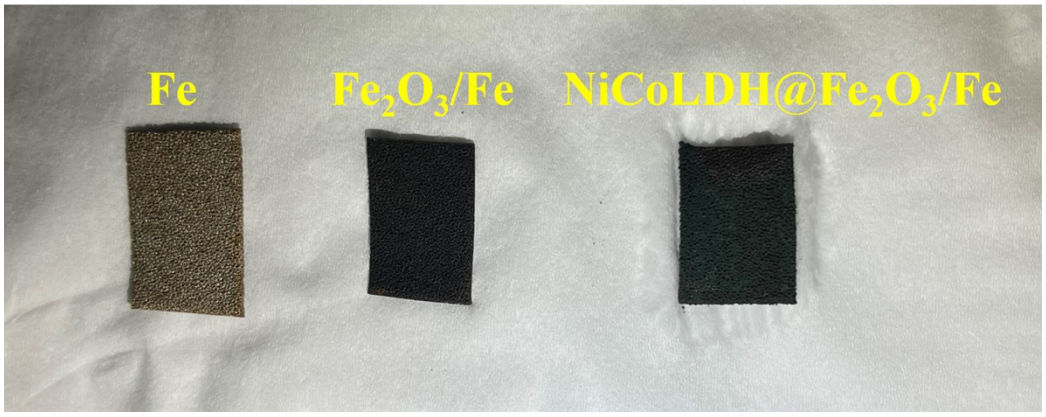

Fig. S4. Photographs showing of Fe foam, Fe_2O_3/Fe and (NiCoLDH@Fe_2O_3/Fe

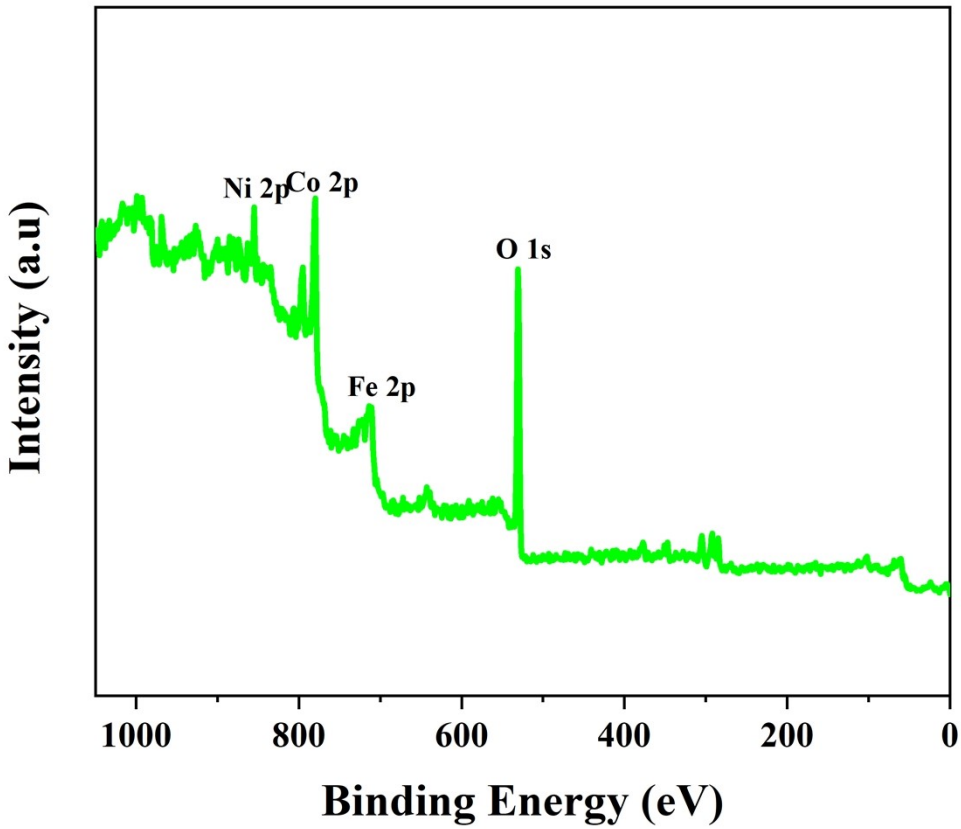

Fig. S5. XPS spectrum of NiCoLDH@Fe_2O_3/Fe

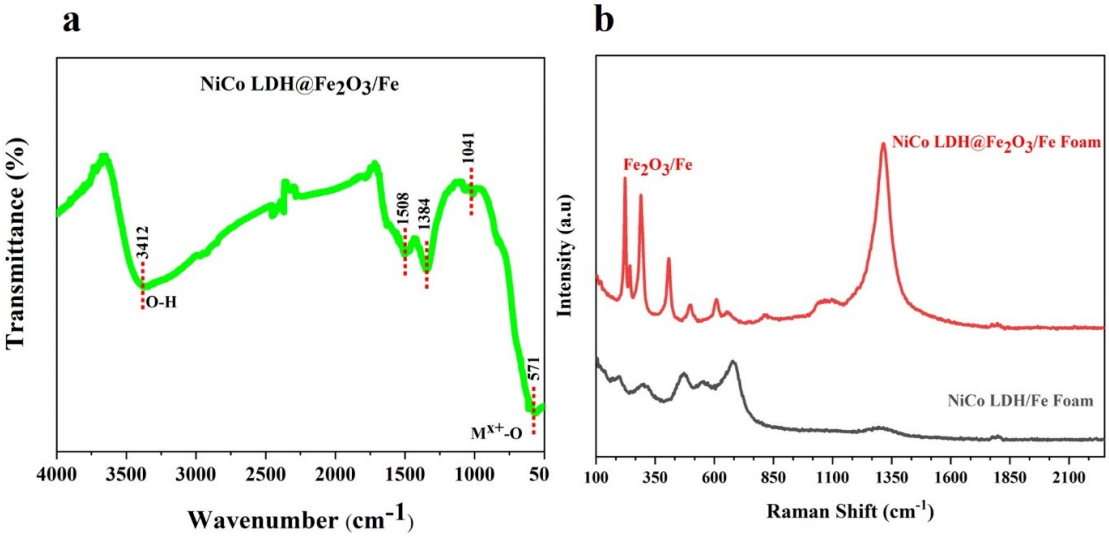

Fig. S6 (a) Fourier transform infrared spectroscopy (FT-IR) analysis (b) Raman spectroscopy

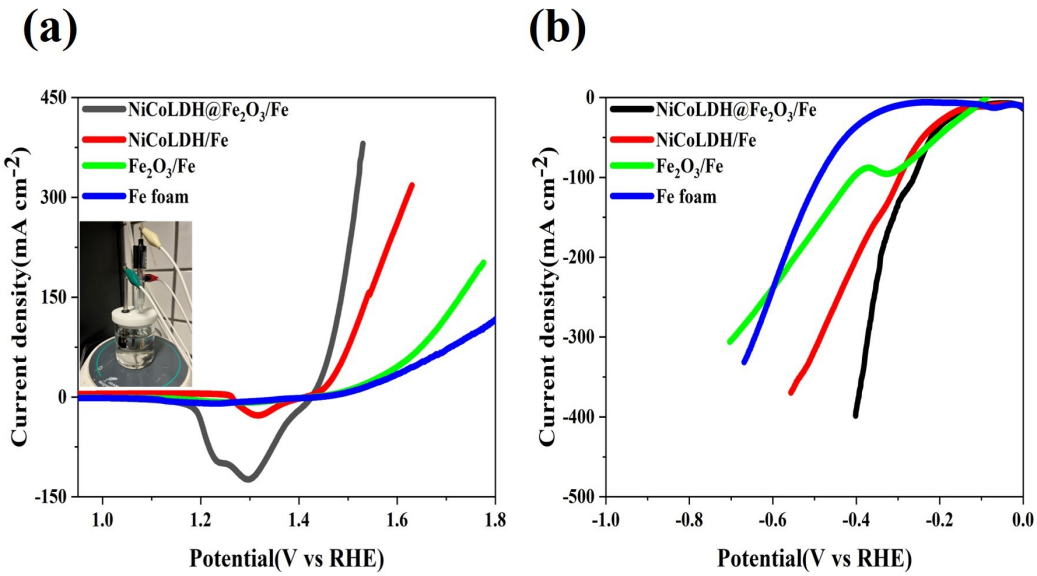

Fig. S7. LSV curves of Fe foam, Fe_2O_3/Fe, (NiCo LDH/Fe and NiCoLDH@Fe_2O_3/Fe for (a) OER and (b) HER in 1.0 M KOH (with iR-compensation).

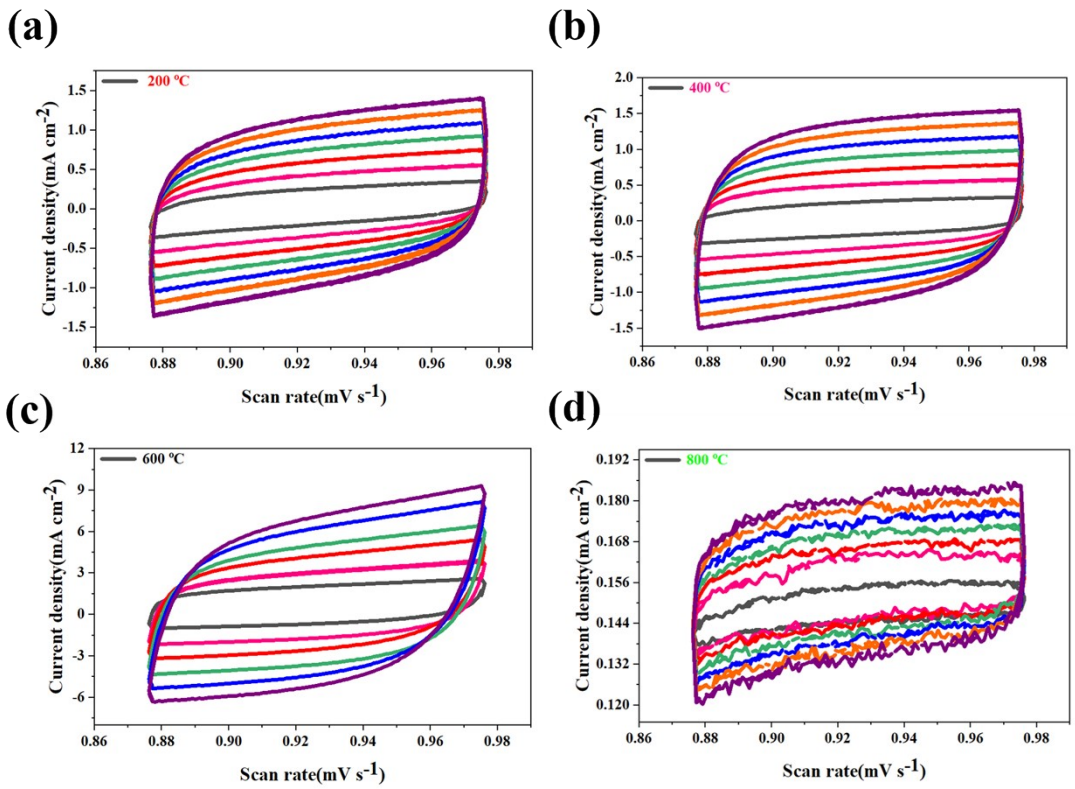

Fig. S8. CV in the region of -0.05 ~ 0.05 V for NiCoLDH@Fe_2O_3/Fe at different temperature for OER.

Fig. S9 and S10 are cyclic voltametric and linear fitting diagrams of NiCoLDH@Fe_2O_3/Fe derived at different temperature, the ECSA of the NiCoLDH@Fe_2O_3/Fe were calculated to be 231.75 cm2, 231.25 cm2, 1550 cm^2 and 5 cm2 respectively when the Temperature was (200 to 800 °C. Because the reason of at 600°C provide a significantly larger surface area and more active catalytic sites compared to bare Fe foam or NiCo LDH alone. At the 600°C provides the right balance between crystal growth, surface area, and stability, making it the optimal temperature for growing highly active Fe_2O_3/Fe nano-whiskers structures for catalytic applications. The combination of well-aligned nano-whiskers with the electrodeposited NiCo LDH layer results in an enhanced structure with superior catalytic performance, making NiCoLDH@Fe_2O_3/Fe highly effective for electrochemical applications. Therefore, this temperature was employed to ensure.

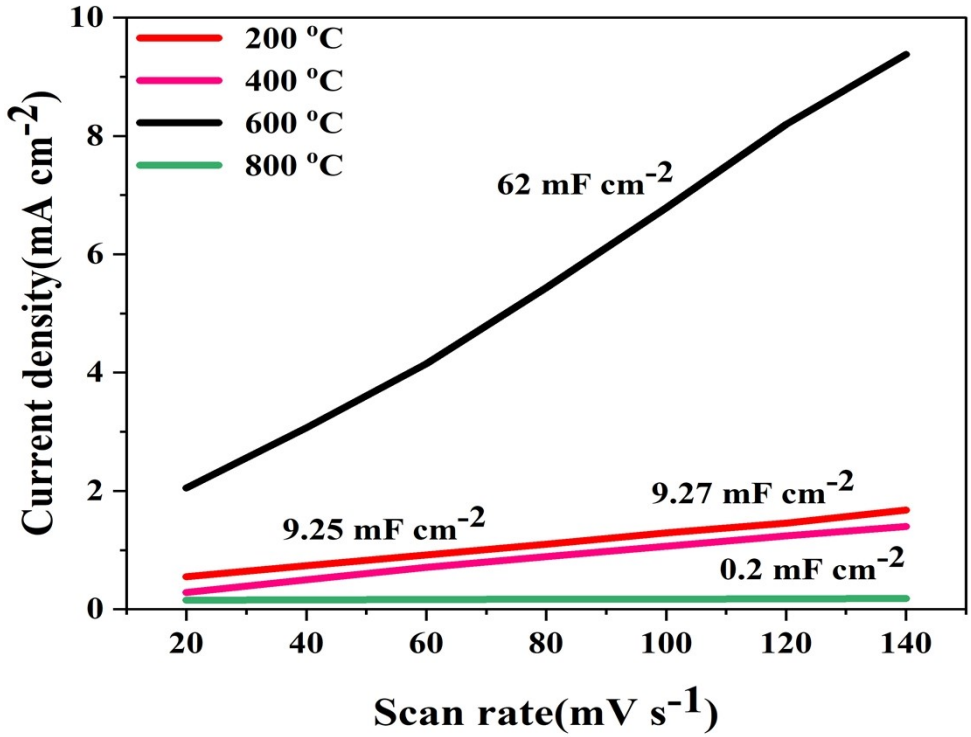

Fig. S9. The Cdl values of NiCoLDH@Fe_2O_3/Fe at the scan rate ws 20 to 140 mV/s Fe prepared at different temperature for OER.

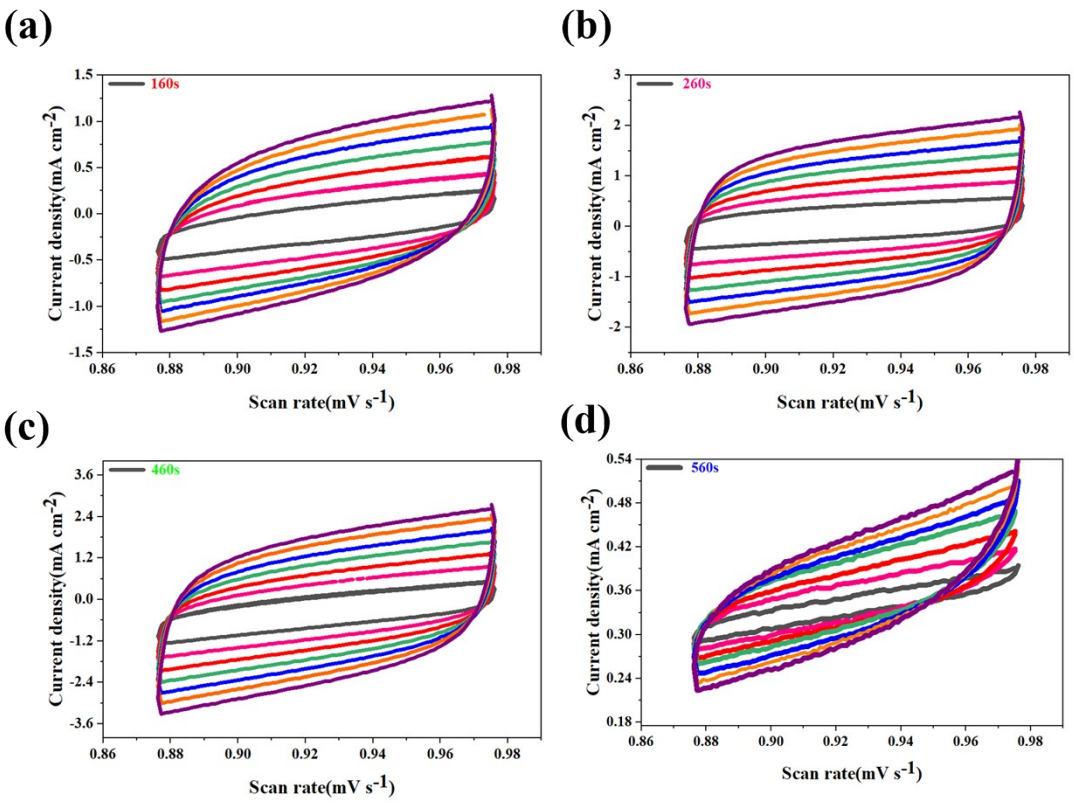

Fig. S10. CV tested in the potential window of -0.05 ~ 0.05 V at scan rates from 20 to 140 mV/s for NiCoLDH@Fe_2O_3/Fe prepared at different deposition of time.

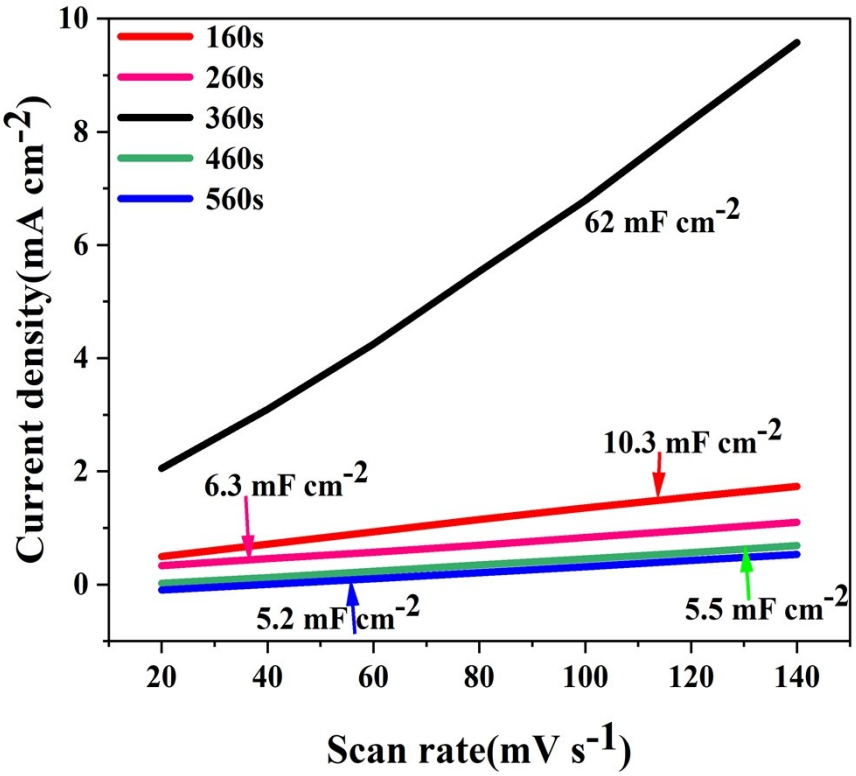

Fig. S11. The Cdl values of NiCoLDH@Fe_2O_3/Fe at the scan rate was 20 to 140 mV/s Fe prepared at different deposition of time for OER.

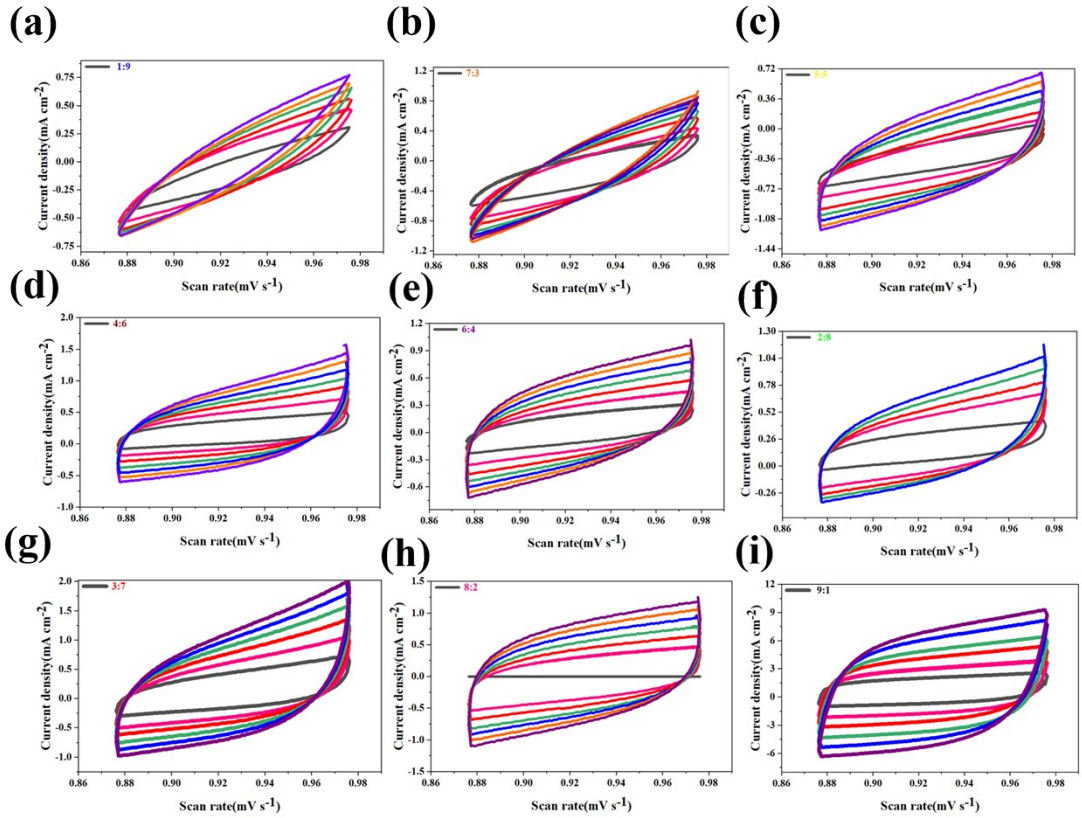

Fig. S12. CV tested in the potential window of -0.05 ~ 0.05 V at scan rates from 20 to 140 mV/s for NiCoLDH@Fe_2O_3/Fe prepared at different ratio base.

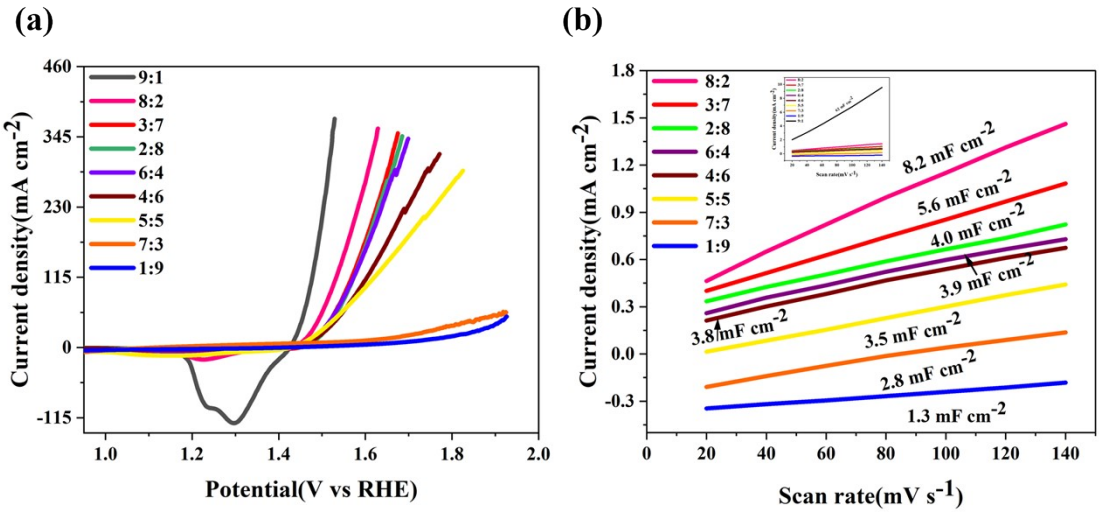

Fig. S13. (a) The LSV and (b) Cdl as a function of the scan rate regarding NiCoLDH@Fe_2O_3/Fe prepared with different ratio base.

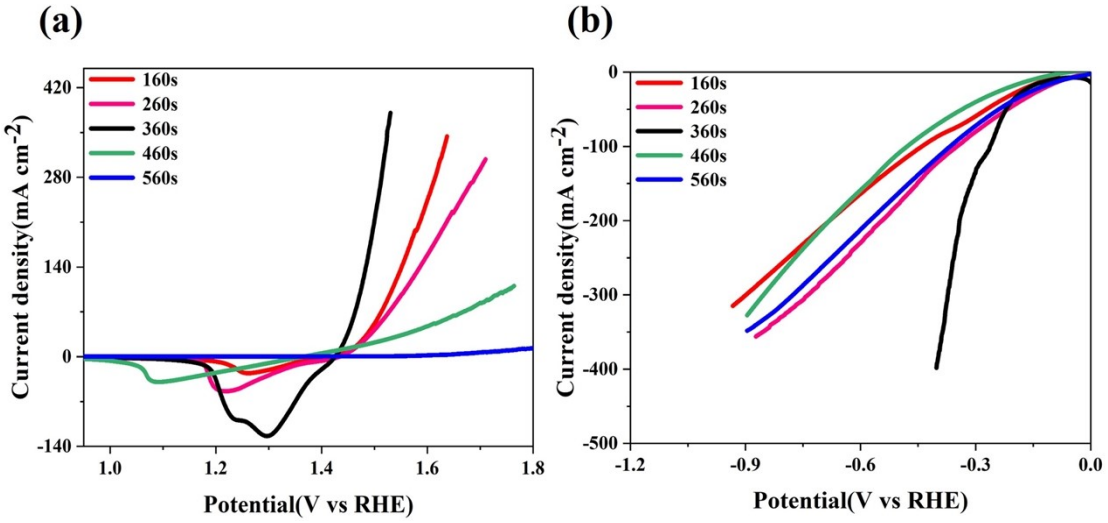

Fig. S14. LSV curves of (NiCo LDH@Fe_2O_3)/Fe prepared with different deposition of time (a) OER and (b) HER in 1.0 M KOH (with iR-compensation).

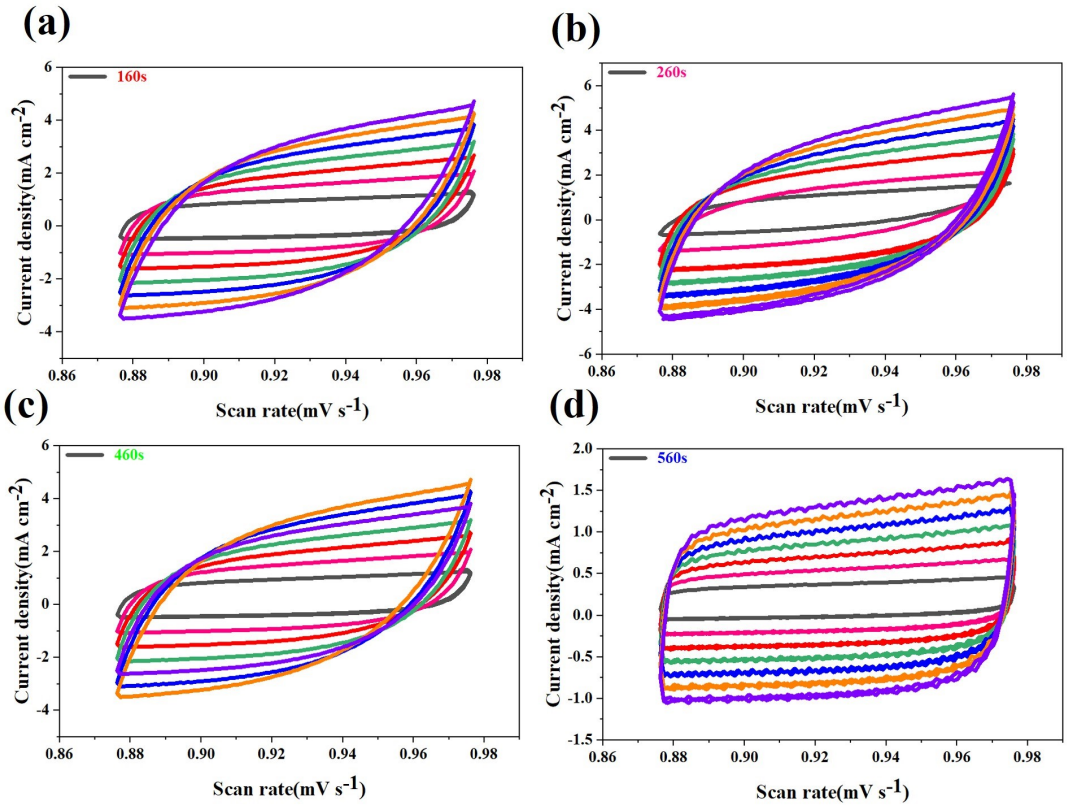

Fig. S15. CV graphs of HER obtained in the potential window of -0.05 ~ 0.05V with NiCoLDH@Fe2O3/Fe prepared at different deposition of time.

As shown in Fig. S14 and S15, and for main at 360s in Fig. S10 leads to larger Cdl and ECSA of the obtained material. Due to the possible reason, at different deposition conditions (160, 260, 360, and 560), the homogeneity and quality of the NiCo LDH layer on Fe_2O_3/Fe. At 160 and 260 insufficient deposition yields thin or uneven layers, reducing active sites and hindering electron transport. Conversely, at 560, excessive deposition produces overly thick layers that block active sites and increase diffusion resistance. The optimal deposition at 360 achieves a precise balance, forming a uniform NiCo LDH layer that effectively coats the Fe_2O_3 nano whiskers while preserving access to active sites, thereby enhancing catalytic efficiency.

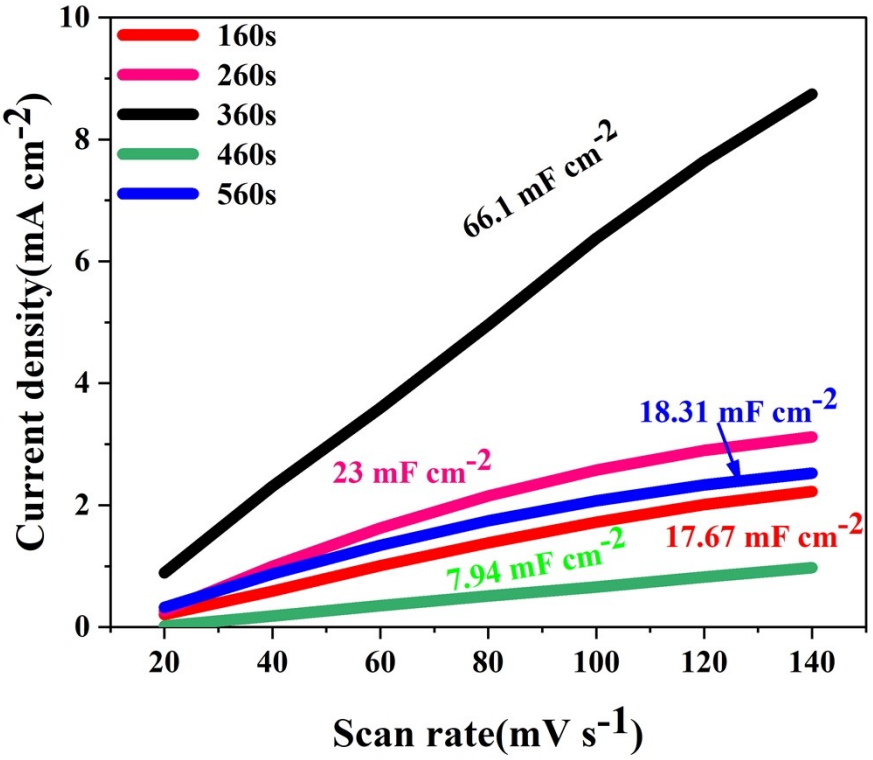

Fig. S16. The Cdl values of HER at -0.05-0.05 potential window as a function of the scan rate of NiCo LDH@Fe_2O_3/Fe prepared with deposition of time.

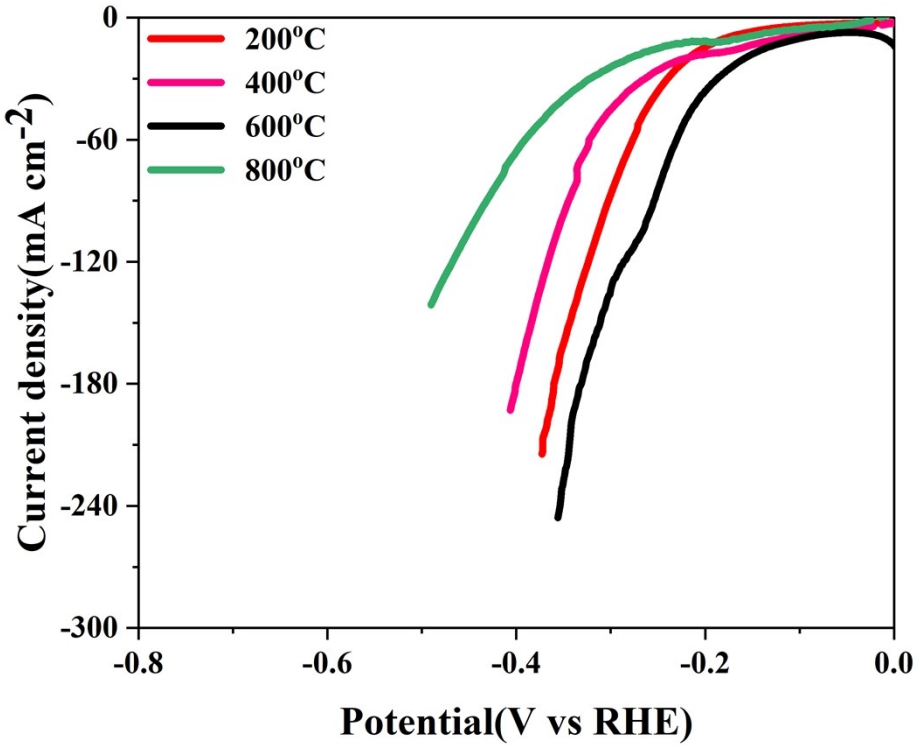

Fig. S17. HER polarization curves of NiCo LDH@Fe_2O_3/Fe at different temperature base in a furnace (with 65% iR-compensation).

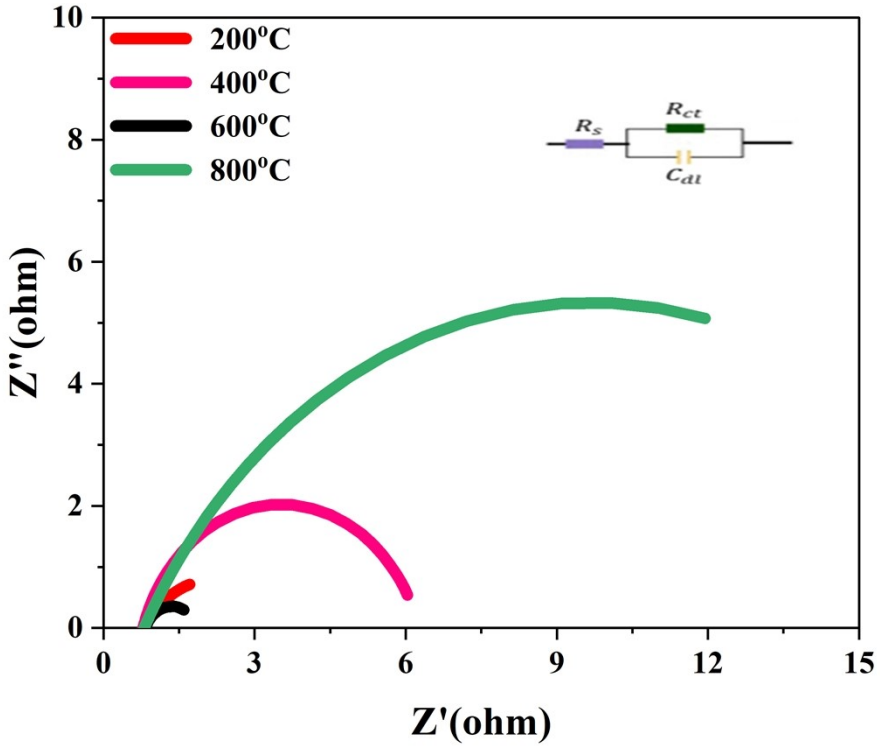

Fig. S18. Nyquist plots of HER at an overpotential of 246 mV of (NiFCoLDH@Fe_2O_3)/Fe at different temperature base.

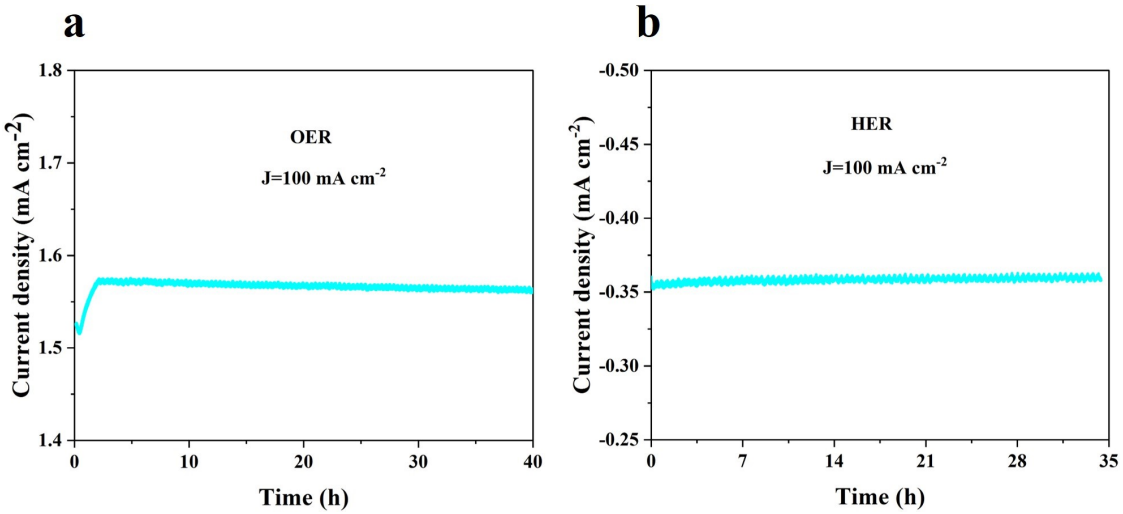

Fig. S19. (a) is the stability test of OER at 100 mA cm-2 (b) is the stability test of the HER in 1 M KOH

In (Fig. S19). In (Fig.19a) The NiCo LDH@Fe_2O_3/Fe electrocatalyst exhibits excellent stability in 1M KOH electrolyte. For the oxygen evolution reaction (OER), it initially requires an overpotential of 1.56 V to achieve a current density of 100 mA cm^{-2}. After 10 hours of continuous operation, the overpotential slightly decreases to 1.54 V, indicating consistent performance without signs of degradation. In (Fig.19b) hydrogen evolution reaction (HER), the catalyst maintains a stable current density of 100 mA cm^{-2} at an overpotential of -0.36 V for over 35 hours, further demonstrating its strong long-term durability.

Table S1. Comparison of overpotentials of different electrode materials at current densities of 10 and 100 mA cm^{-2} for hydrogen evolution reaction in 1 M KOH at room temperature

Electrode material	HER η_{10} (mV)	η_{100} (mV)	Tafel slope (mV dec^{-1})	References
(NiCo LDH@Fe_2O_3)/Fe	**96**	**256**	**54.7**	**This work**
(NiFe LDH@NiCoP/NF)	102	N/A	43	[1]
NiFeNb-0.25/NF	207	N/A	98.7	[2]
N-doped NiCo LDH (N-NiCo LDH)	100	N/A	42	[3]
NiCo-LDH-OH	180	N/A	74.38	[4]
Co0.03-NiFe0.97 LDHs	170	N/A	96	[5]
Ce-doped NiFe-LDH	147	N/A	45	[6]
P-V-NiFe LDH NSA	134	N/A	37.2	[7]
Co_3Fe1-LDH/rGO/NF	110	N/A	60	[8]
W doped NiO/NiS_2	116	N/A	31.5	[9]
Mo-Co_9Se_8/FeNiSe	108	N/A	36	[10]
MnFe-LDH	120	N/A	86	[11]
NiFePx	112	N/A	26.1	[12]
Ru-Fe_3O_4@FeNi-LDH/IF	104	N/A	86.5	[13]
NiFe LDH/Fe_2O_3/Ni_3S_2/IF		162	170	[14]
Ni/NiFe-LDH/IF	56	N/A	68	[15]

Table S2. Comparison of overpotentials of different electrode materials at current densities of 10 and 100 mA cm^{-2} as well as Tafel plot for oxygen evolution reaction(OER) in 1 M KOH at room temperature

Electrode material	OER η_{10} (mV)	η_{100} (mV)	Tafel slope (mV dec^{-1})	References
(NiCo LDH@Fe_2O_3)/Fe	**202**	**241**	**40**	**This work**
NiCoFe-P/C	257	N/A	20	[1, 16]
$NiSe_2$@Fe-NiCo LDH	260	200	58.56	[1]
CoNi/$CoNiO_2$@NC-600/CC	N/A	263	63	[17]
Fe-doped (Ni, Mn) Co_2O_4	242	N/A	78.9	[18]
Ni_3Se_2@NiFe-LDH/NF	222	N/A	61.3	[19]
$SrNiO_3$ nanoparticles	259	N/A	70	[20]
2-APSC/NF	N/A	292	N/A	[21]
Ni_2P@C/NF-12 h	N/A	294	63	[22]
NiCo-LDH-OH	317	N/A	115.76	[4]
NGCNC	N/A	300	42	[23]
$Ni_2CoFe0.5$-LDH/NF	240	N/A	65	[24]
Cu@GDY -Co	N/A	304	51.7	[25]
NiFe RTNC/CW	N/A	309	N/A	[26]
CoNiN@NiFe LDH	227	291	N/A	[27]
Ni_3S_2/VG@NiCo LDHs	N/A	350	65	[28]
CNTs@IreCoNi_2S_4 NSs	N/A	362	148.8	[29]
Co3Fe1-LDH/rGO/NF	250	N/A	43	[8]
(NixFeyCo_6-x-y) Mo6C,	212	N/A	55.1	[30]

NiCoP/NF	253	N/A	49.5	[31]
Fe_3C@CNOs	N/A	400	48.9	[32]
NG-NiFe@MoC_2-2	N/A	412	31	[33]
W doped NiO/NiS_2	263	N/A	73.4	[9]
MoNi(OH)2/FexNiy(OH)3x+2y	229	268	33.53	[34]
MnFe-LDH	280	N/A	92	[11]
CoO@S-CoTe	246	N/A	56	[35]
$NiFeWO_4$@NiFe-LDH/G	N/A	440	32.1	[36]
NiFe-LDH@IF-200-72 NiFe LDH/IF		209	25.6	[37]
NiFe LDH/Fe_2O_3/Ni_3S_2/IF		226.2	59.1	[14]
Ni/NiFe-LDH/IF		140	77.0	[15]
Ru-Fe_3O_4@FeNi-LDH/IF		189	34	[13]

Table S3. Comparison of cell voltages of different electrode materials at current densities of 100 and 500 mA cm^{-2} for overall water splitting (OWS) under industrial testing condition (6 M or 30wt% KOH 60-80 ^{o}C)

Electrode material	Cell voltage at 100 mA/cm^2 (V)	Cell voltage at 500 mA/cm^2 (V)	References
NiCoLDH@Fe_2O_3|| NiCoLDH@Fe_2O_3	**1.58**	**1.8**	**This work**
CoFe-Ni_2P||CoFe-Ni_2P	N/A	1.8	[38]
Fe-Ni_3S_2/PNF-5||Fe-Ni_3S_2/PNF-5	N/A	1.81	[39]
($CoNi_2S_4$@NiMn LDH/SCC) ||($CoNi_2S_4$@NiMn LDH/SCC)	1.69	N/A	[40]
Fe_2P-WO2.92/NF|| Fe_2P-WO2.92/NF	N/A	1.95	[41]
(Ni/MoO_2@CN) ||(Ni/MoO_2@CN)	N/A	1.92	[42]
3D Fe0−NixSy/NF||3D Fe0−NixSy/NF	N/A	2.4	[43]
Co_3Fe1-LDH/rGO/NF|| Co_3Fe1-LDH/rGO/NF	1.84	N/A	[8]
Ni3P/MnOOH|| Ni3P/MnOOH	N/A	2	[44]
Ni/MoO_2@CN||Ni/MoO_2@CN	N/A	1.81	[45]
SCI-350/NF||SCI-350/NF	N/A	1.84	[46]
Ni-B-P||Ni-B-P	N/A	1.88	[47]
Ni/MoN/rNS||Ni/MoN/rNS	N/A	2.8	[48]
NiO/α-Fe_2O_3@NF|| NiO/α-Fe_2O_3@NF	N/A	1.99	[49]
$NiFe_2O_4$/NiFe LDH|| $NiFe_2O_4$/NiFe LDH	N/A	1.93	[50]
Fe_2O_3@Ni_2P/$Ni(PO_3)_2$/NF|| Fe_2O_3@Ni_2P/$Ni(PO_3)_2$/NF	1.93	2.48	[51]

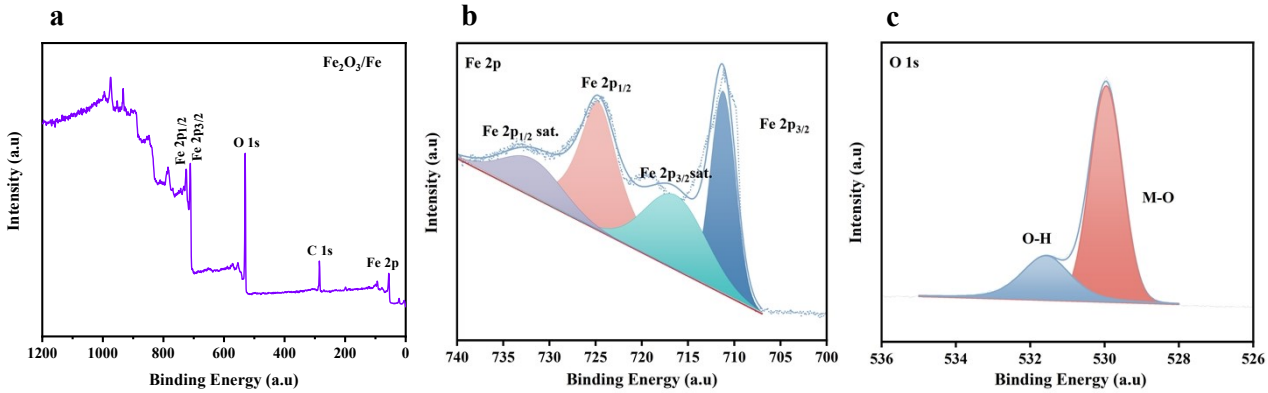

Fig. S20 (a) is the XPS survey of Fe_2O_3/ Fe (b,c) is the high-resolution spectra of Fe 2p and O1s

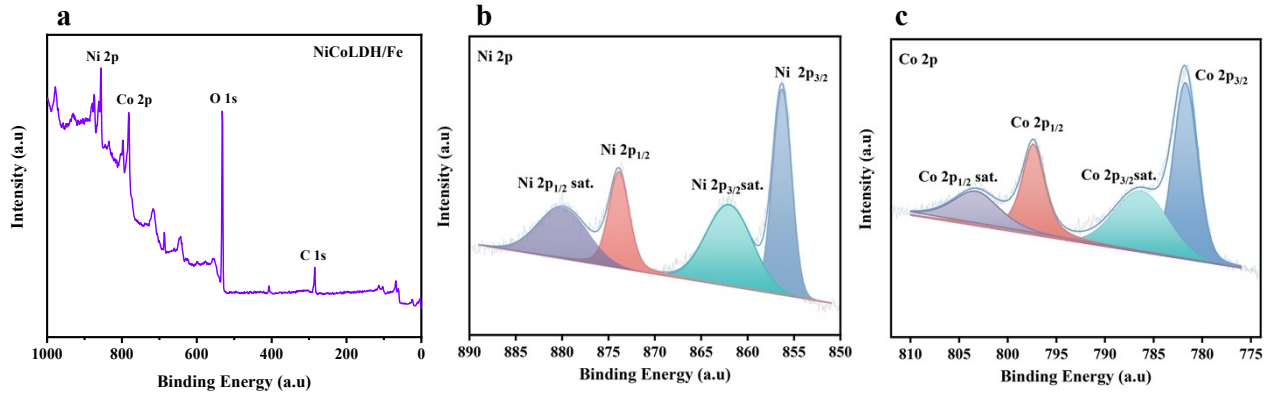

Fig. S21 (a) is the XPS survey of NiCo/Fe (b,c) is the high-resolution spectra of Ni 2p and Co 2p

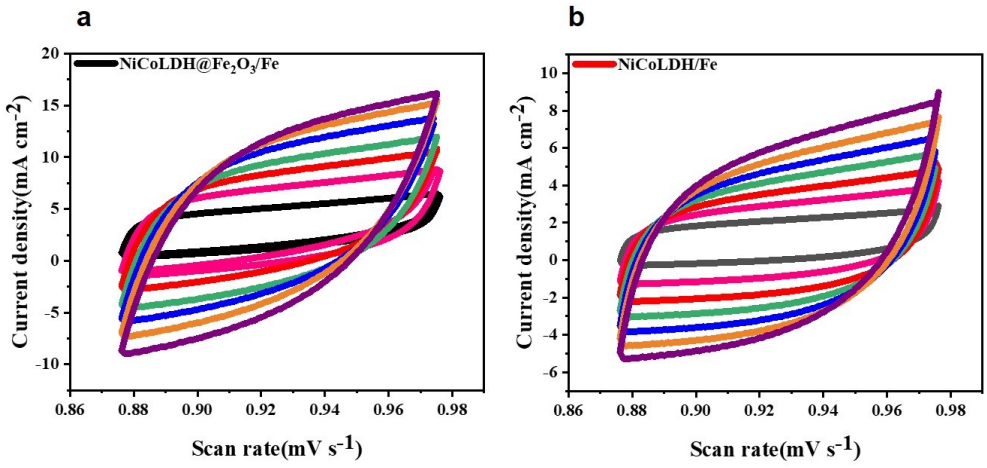

Fig. S22 (a) is the CV of NiCo LDH@Fe_2O_3/Fe (b,) is the CV of NiCo LDH/Fe

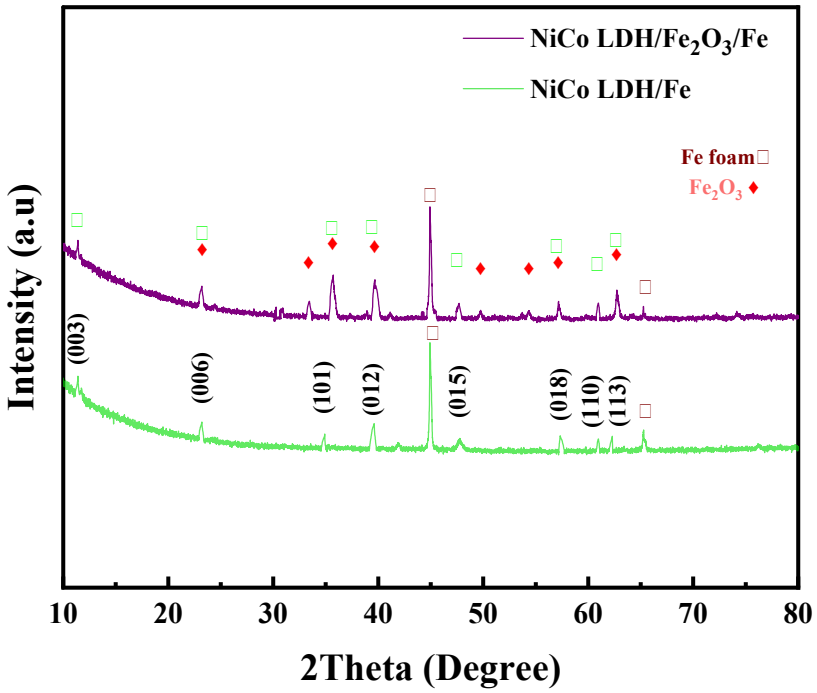

Fig. S23 XRD electrocatalyst after stability test

Table S4 C_{dl} & ECSA of OWS

Electrocatalyst	C_{dl} (mF cm^{-2})	ECSA (cm^2)
NiCo LDH@ Fe_2O_3/Fe	124	3100
NiCo LDH/Fe	64.3	1607
Fe_2O_3/Fe	5.8	145

Table S5 Comparison of stability test of different electrode materials at current densities of 100 mA cm^{-2} for overall water splitting under industrial testing condition (6 M KOH at room temperature 25 ^{o}C)

Electrode material	Current density (mA cm^{-2})	Electrolyte	Durability test (time in h)	References
NiCoLDH@Fe_2O_3	**100**	**1.0 M KOH**	**120**	**This work**
$CoMoO_4$	100	1.0 M KOH	80	[52]
$Ni(PO_3)_2$-CoP_4/$CoMoO_4$/NF (−)	100	1.0 M KOH	60	[53]
Mo-NiPx/NiSy	100	1.0 M KOH	27	[54]
$CoMoO_4$-CoP/NC	100	1.0 M KOH	30	[55]
CoNiP/CoNiFeP@NCNFs	100	1.0 M KOH	24	[56]
Ni_2P-Fe_2P	100	1.0 M KOH	48	[57]
Ru-NiCoP/NF	100	1.0 M KOH	50	[58]
n-FeO||p-α-Fe_2O_3 NPs	100	1.0 M KOH	80	[59]
$Fe(OH)_3$–3/Ni-NiO/CC	100	1.0 M KOH	40	[60]
Ni_5Mo/$NiCo_2O_4$	100	1.0 M KOH	50	[61]
CoO/MoO_x	100	1.0 M KOH	10	[62]

References

[1] X. Chen, X. Yu, C. Yang, G. Wang, Enhancing OER and overall water splitting performance of amorphous NiFe LDH grown on Ni foam with the needle-like NiCoP transition layer, Journal of Solid State Chemistry, 333 (2024) 124649.

[2] A. Gupta, H.K. Sadhanala, A. Gedanken, Iron doped cobalt nickel layered double hydroxide supported on nickel foam as a robust electrocatalyst for highly efficient water oxidation in alkaline sea water, Electrochimica Acta, 470 (2023) 143269.

[3] T. Chen, R. Zhang, G. Chen, J. Huang, W. Chen, X. Wang, D. Chen, C. Li, K.K. Ostrikov, Plasma-doping-enhanced overall water splitting: case study of NiCo hydroxide electrocatalyst, Catalysis Today, 337 (2019) 147-154.

[4] H. Yang, Z. Zhou, H. Yu, H. Wen, R. Yang, S. Peng, M. Sun, L. Yu, Alkali treatment of layered double hydroxide nanosheets as highly efficient bifunctional electrocatalysts for overall water splitting, Journal of Colloid and Interface Science, 636 (2023) 11-20.

[5] Y. Ye, H. Li, J. Cao, X. Liu, H. Fan, M. Wei, L. Yang, J. Yang, Y. Chen, Constructing microstructures in nickel-iron layered double hydroxide electrocatalysts by cobalt doping for efficient overall water splitting, International Journal of Hydrogen Energy, 48 (2023) 17026-17034.

[6] H.S. Jadhav, A. Roy, B.Z. Desalegan, J.G. Seo, An advanced and highly efficient Ce assisted NiFe-LDH electrocatalyst for overall water splitting, Sustainable Energy & Fuels, 4 (2020) 312-323.

[7] X. Zhang, Y. Qiu, Q. Li, F. Liu, L. Cui, C. Li, J. Liu, Sandwich structured Fe3O4/NiFe LDH/Fe3O4 as a bifunctional electrocatalyst with superior stability for highly sustained overall water splitting, Journal of Alloys and Compounds, 932 (2023) 167612.

[8] J. Guo, Z. Wei, K. Wang, H. Zhang, Synergistic coupling of CoFe-layered double hydroxide nanosheet arrays with reduced graphene oxide modified Ni foam for highly efficient oxygen evolution reaction and hydrogen evolution reaction, International Journal of Hydrogen Energy, 46 (2021) 27529-27542.

[9] H. Wang, T. Liu, K. Bao, J. Cao, J. Feng, J. Qi, W doping dominated NiO/NiS2 interfaced nanosheets for highly efficient overall water splitting, Journal of colloid and interface science, 562 (2020) 363-369.

[10] J. Liang, S. Li, F. Li, L. Zhang, Y. Jiang, H. Ma, K. Cheng, L. Qing, Defect engineering induces Mo-regulated Co9Se8/FeNiSe heterostructures with selenium vacancy for enhanced electrocatalytic overall water splitting in alkaline, Journal of Colloid and Interface Science, 655 (2024) 296-306.

[11] A. Mariappan, R.K. Dharman, T.H. Oh, S. Prabu, K.-Y. Chiang, Construction of MnFe layer double hydroxide on biomass-derived carbon heterostructure for efficient electrocatalytic water splitting, Materials Chemistry and Physics, 309 (2023) 128321.

[12] J. Zhao, N. Liao, J. Luo, Transforming NiFe layered double hydroxide into NiFeP x for efficient alkaline water splitting, Journal of Materials Chemistry A, 11 (2023) 9682-9690.

[13] L. Ye, Y. Zhang, B. Guo, D. Cao, Y. Gong, Ru doping induces the construction of a unique core–shell microflower self-supporting electrocatalyst for highly efficient overall water splitting, Dalton Transactions, 50 (2021) 13951-13960.

[14] D. Deng, Q. Li, S. Lei, W. Zhang, H. Li, L. Xu, NiFe LDH/Fe2O3/Ni3S2 heterostructure with a superhydrophilic/superaerophobic surface for solar-driven electrolytic water splitting, Inorganic Chemistry, 63 (2024) 20022-20029.
[15] Y. Liu, J. Mao, Y. Yuan, H. Huang, X. Ma, X. Li, Z. Jin, Accelerating corrosion of iron foam enables a bifunctional catalyst for overall water splitting, Materials Chemistry Frontiers, 7 (2023) 5858-5867.
[16] R. Liu, X.-R. Shi, Y. Wen, X. Shao, C. Su, J. Hu, S. Xu, Trimetallic synergistic optimization of 0D NiCoFe-P QDs anchoring on 2D porous carbon for efficient electrocatalysis and high-energy supercapacitor, Journal of Energy Chemistry, 74 (2022) 149-158.
[17] Q. Zhang, X.L. Li, B.X. Tao, X.H. Wang, Y.H. Deng, X.Y. Gu, L.J. Li, W. Xiao, N.B. Li, H.Q. Luo, CoNi based alloy/oxides@N-doped carbon core-shell dendrites as complementary water splitting electrocatalysts with significantly enhanced catalytic efficiency, Applied Catalysis B-Environmental, 254 (2019) 634-646.
[18] H. Shi, Q. Zha, Y. Ni, Fe-doped (Ni, Mn) Co2O4 nanorod arrays on Ni foam as highly efficient electrocatalyst for oxygen evolution reaction in alkaline and neutral conditions with superb long-term stability, Journal of Alloys and Compounds, 904 (2022) 164052.
[19] J. Hu, S. Zhu, Y. Liang, S. Wu, Z. Li, S. Luo, Z. Cui, Self-supported Ni3Se2@ NiFe layered double hydroxide bifunctional electrocatalyst for overall water splitting, Journal of colloid and interface science, 587 (2021) 79-89.
[20] J. Junita, D. Jayalakshmi, J.D. Rodney, Effect of annealing temperature on the bifunctional electrocatalytic properties of strontium nickelate (SrNiO3) nanoparticles for efficient overall water splitting, International Journal of Hydrogen Energy, 47 (2022) 30602-30612.
[21] Y. Zhang, J. Yang, Z. Yu, Y. Hou, R. Jiang, J. Huang, F. Yang, S. Yao, L. Gao, W. Tang, Modulating carbon-supported transition metal oxide by electron-giving and electron-absorbing functional groups towards efficient overall water splitting, Chemical Engineering Journal, 416 (2021).
[22] N. Chen, S. Che, H. Liu, G. Li, N. Ta, F.J. Chen, B. Jiang, N. Wu, Z. Li, W. Yu, F. Yang, Y. Li, Multistage interfacial engineering of 3D carbonaceous Ni2P nanospheres/nanoflowers derived from Ni-BTC metal-organic frameworks for overall water splitting, Journal of Colloid and Interface Science, 638 (2023) 582-594.
[23] S. Riyajuddin, K. Azmi, M. Pahuja, S. Kumar, T. Maruyama, C. Bera, K. Ghosh, Super-Hydrophilic Hierarchical Ni-Foam-Graphene-Carbon Nanotubes-Ni2P-CuP2 Nano-Architecture as Efficient Electrocatalyst for Overall Water Splitting, ACS Nano, 15 (2021) 5586-5599.
[24] Q. Ma, B. Li, F. Huang, Q. Pang, Y. Chen, J.Z. Zhang, Incorporating iron in nickel cobalt layered double hydroxide nanosheet arrays as efficient oxygen evolution electrocatalyst, Electrochimica Acta, 317 (2019) 684-693.
[25] G. Shi, Y. Xie, L. Du, Z. Fan, X. Chen, X. Fu, W. Xie, M. Wang, M. Yuan, Stabilization of cobalt clusters with graphdiyne enabling efficient overall water splitting, Nano Energy, 74 (2020).
[26] X. Sheng, Y. Li, T. Yang, B.J.J. Timmer, T. Willhammar, O. Cheung, L. Li, C.J. Brett, S.V. Roth, B. Zhang, L. Fan, Y. Guo, X. Zou, L. Berglund, L. Sun, Hierarchical micro-reactor as electrodes for water splitting by metal rod tipped carbon nanocapsule self-assembly in carbonized wood, Applied Catalysis B-Environmental, 264 (2020).
[27] J. Wang, G. Lv, C. Wang, A highly efficient and robust hybrid structure of CoNiN@ NiFe LDH for overall water splitting by accelerating hydrogen evolution kinetics on NiFe LDH, Applied Surface Science, 570 (2021) 151182.

[28] X. Zhang, J. Fan, X. Lu, Z. Han, C. Cazorla, L. Hu, T. Wu, D. Chu, Bridging NiCo layered double hydroxides and Ni3S2 for bifunctional electrocatalysts: The role of vertical graphene, Chemical Engineering Journal, 415 (2021).
[29] X. Zhu, D.C. Nguyen, S. Prabhakaran, D.H. Kim, N.H. Kim, J.H. Lee, Activating catalytic behavior of binary transition metal sulfide-shelled carbon nanotubes by iridium incorporation toward efficient overall water splitting, Materials Today Nano, 21 (2023).
[30] L.-G. He, P.-Y. Cheng, C.-C. Cheng, C.-L. Huang, C.-T. Hsieh, S.-Y. Lu, (NixFeyCo6-xy) Mo6C cuboids as outstanding bifunctional electrocatalysts for overall water splitting, Applied Catalysis B: Environmental, 290 (2021) 120049.
[31] H.-S. Hu, Y. Li, Y.-R. Shao, K.-X. Li, G. Deng, C.-B. Wang, Y.-Y. Feng, NiCoP nanorod arrays as high-performance bifunctional electrocatalyst for overall water splitting at high current densities, Journal of Power Sources, 484 (2021) 229269.
[32] S. Xu, M. Wang, G. Saranya, N. Chen, L. Zhang, Y. He, L. Wu, Y. Gong, Z. Yao, G. Wang, Z. Wang, S. Zhao, H. Tang, M. Chen, H. Gou, Pressure-driven catalyst synthesis of Co-doped Fe3C@Carbon nano-onions for efficient oxygen evolution reaction, Applied Catalysis B-Environmental, 268 (2020).
[33] Q. Hu, X. Liu, B. Zhu, L. Fan, X. Chai, Q. Zhang, J. Liu, C. He, Z. Lin, Crafting MoC2-doped bimetallic alloy nanoparticles encapsulated within N-doped graphene as roust bifunctional electrocatalysts for overall water splitting, Nano Energy, 50 (2018) 212-219.
[34] Y. Liu, M. Ding, Y. Qin, B. Zhang, Y. Zhang, J. Huang, Crystalline/Amorphous Mo-Ni (OH) 2/FexNiy (OH) 3x+ 2y hierarchical nanotubes as efficient electrocatalyst for overall water splitting, Journal of Colloid and Interface Science, 657 (2024) 219-228.
[35] X. Wang, Z. Mao, X. Mao, X. Hu, F. Gao, M. Gao, Q.L. Wu, X. Lyu, A. Du, X. Xu, Dual integrating oxygen and sulphur on surface of CoTe nanorods triggers enhanced oxygen evolution reaction, Advanced Science, 10 (2023) 2206204.
[36] S. Song, Y. Fu, F. Yin, Y. Zhang, J. Ma, Y. Liu, J. Ren, W. Ye, R. Ma, NiFe-based tungstate@layered double hydroxide heterostructure supported on graphene as efficient oxygen evolution reaction catalyst, Materials Today Chemistry, 28 (2023).
[37] W. Zhao, H. Xu, H. Luan, N. Chen, P. Gong, K. Yao, Y. Shen, Y. Shao, NiFe Layered Double Hydroxides Grown on a Corrosion-Cell Cathode for Oxygen Evolution Electrocatalysis (Adv. Energy Mater. 2/2022), Advanced Energy Materials, 12 (2022).
[38] C. Huang, Q. Zhou, L. Yu, D. Duan, T. Cao, S. Qiu, Z. Wang, J. Guo, Y. Xie, L. Li, Y. Yu, Functional Bimetal Co-Modification for Boosting Large-Current-Density Seawater Electrolysis by Inhibiting Adsorption of Chloride Ions, Advanced Energy Materials, 13 (2023) 2301475.
[39] B. Zhong, B. Cheng, Y. Zhu, R. Ding, P. Kuang, J. Yu, Hierarchically porous nickel foam supported Fe-Ni3S2 electrode for high-current-density alkaline water splitting, Journal of Colloid and Interface Science, 629 (2023) 846-853.
[40] P. Wang, J. Qi, C. Li, W. Li, T. Wang, C. Liang, Hierarchical CoNi2S4@ NiMn-layered double hydroxide heterostructure nanoarrays on superhydrophilic carbon cloth for enhanced overall water splitting, Electrochimica Acta, 345 (2020) 136247.
[41] Q. Peng, Q. He, Y. Hu, T.T. Isimjan, R. Hou, X. Yang, Interface engineering of porous Fe2P-WO2. 92 catalyst with oxygen vacancies for highly active and stable large-current oxygen evolution and overall water splitting, Journal of Energy Chemistry, 65 (2022) 574-582.
[42] Z. Zhang, J. Zhao, M. Wu, Q. Lu, R. Liu, Three-phase interface induced charge modulation on

MoO2/Mo2C-carbon tube for enhanced hydrogen evolution, Nano Research, 16 (2023) 4706-4714.
[43] X. Cheng, C. Lei, J. Yang, B. Yang, Z. Li, J. Lu, X. Zhang, L. Lei, Y. Hou, K. Ostrikov, Efficient Electrocatalytic Oxygen Evolution at Extremely High Current Density over 3D Ultrasmall Zero-Valent Iron-Coupled Nickel Sulfide Nanosheets, ChemElectroChem, 5 (2018) 3866-3872.
[44] Y. Tan, Q. Li, Q. Che, X. Chen, X. Xu, Y. Chen, Improving activity of Ni3P/Mn hybrid film via electrochemical tuning for water splitting under simulated industrial environment, Electrochimica Acta, 324 (2019) 134897.
[45] G. Qian, J. Chen, T. Yu, J. Liu, L. Luo, S. Yin, Three-Phase Heterojunction NiMo-Based Nano-Needle for Water Splitting at Industrial Alkaline Condition, Nano-Micro Letters, 14 (2022).
[46] H. Guo, Y. Yang, G. Yang, X. Cao, N. Yan, Z. Li, E. Chen, L. Tang, M. Peng, L. Shi, S. Xie, H. Tao, C. Xu, Y. Zhu, X. Fu, Y. Pan, N. Chen, J. Lin, X. Tu, Z. Shao, Y. Sun, Ex Situ Reconstruction-Shaped Ir/CoO/Perovskite Heterojunction for Boosted Water Oxidation Reaction, ACS Catalysis, 13 (2023) 5007-5019.
[47] M.A. Habib, R. Mandavkar, S. Lin, S. Burse, T. Khalid, M.H. Joni, J.-H. Jeong, J. Lee, Ni-B-P micro spheres for superior water splitting OER electrocatalyst satisfying industrial operational requirement, Chemical Engineering Journal, 462 (2023).
[48] Y. Chen, Y. Wang, J. Yu, G. Xiong, H. Niu, Y. Li, D. Sun, X. Zhang, H. Liu, W. Zhou, Underfocus Laser Induced Ni Nanoparticles Embedded Metallic MoN Microrods as Patterned Electrode for Efficient Overall Water Splitting, Advanced Science, 9 (2022) 2105869.
[49] X.-F. Chuah, C.-T. Hsieh, C.-L. Huang, D. Senthil Raja, H.-W. Lin, S.-Y. Lu, In-situ grown, passivator-modulated anodization derived synergistically well-mixed Ni–Fe oxides from Ni foam as high-performance oxygen evolution reaction electrocatalyst, ACS Applied Energy Materials, 2 (2018) 743-753.
[50] X. Zhang, Y. Qiu, Q. Li, F. Liu, X. Ji, J. Liu, Facile construction of well-defined hierarchical NiFe2O4/NiFe layered double hydroxides with a built-in electric field for accelerating water splitting at the high current density, International Journal of Hydrogen Energy, 47 (2022) 40826-40834.
[51] X. Cheng, Z. Pan, C. Lei, Y. Jin, B. Yang, Z. Li, X. Zhang, L. Lei, C. Yuan, Y. Hou, A strongly coupled 3D ternary Fe 2 O 3@ Ni 2 P/Ni (PO 3) 2 hybrid for enhanced electrocatalytic oxygen evolution at ultra-high current densities, Journal of Materials Chemistry A, 7 (2019) 965-971.
[52] J. Fan, X. Chang, L. Li, M. Zhang, Synthesis of CoMoO(4) Nanofibers by Electrospinning as Efficient Electrocatalyst for Overall Water Splitting, Molecules, 29 (2023).
[53] M. Yang, S. Zhang, T. Wang, B. Shi, J. Liu, Y. Tang, Z. Xu, M.T. Sarwar, A. Tang, H. Yang, Multiple Interface Ni(PO3)2-CoP4/CoMoO4 Nanorods for Highly Efficient Hydrogen Evolution in Alkaline Water/Seawater Electrolysis, ACS Sustainable Chemistry & Engineering, 10 (2022) 12423-12432.
[54] J. Wang, M. Zhang, G. Yang, W. Song, W. Zhong, X. Wang, M. Wang, T. Sun, Y. Tang, Heterogeneous Bimetallic Mo-NiPx/NiSy as a Highly Efficient Electrocatalyst for Robust Overall Water Splitting, Advanced Functional Materials, 31 (2021).
[55] J. Luo, Y. Zhou, X. Wang, Y. Gu, W. Liu, S. Wang, J. Zhang, CoMoO4-CoP/NC heterostructure anchored on hollow polyhedral N-doped carbon skeleton for efficient water splitting, Journal of Colloid and Interface Science, 648 (2023) 90-101.
[56] L. Zhi, M. Zhang, J. Tu, M. Li, J. Liu, Coordination polymer and layered double hydroxide dual-precursors derived polymetallic phosphides confined in N-doped hierarchical porous carbon nanoflower as a highly efficient bifunctional electrocatalyst for overall water splitting, Journal of

Colloid and Interface Science, 659 (2024) 82-93.
[57] L. Wu, L. Yu, F. Zhang, B. McElhenny, D. Luo, A. Karim, S. Chen, Z. Ren, Heterogeneous Bimetallic Phosphide Ni2P-Fe2P as an Efficient Bifunctional Catalyst for Water/Seawater Splitting, Advanced Functional Materials, 31 (2020).
[58] D. Chen, R. Lu, Z. Pu, J. Zhu, H.-W. Li, F. Liu, S. Hu, X. Luo, J. Wu, Y. Zhao, S. Mu, Ru-doped 3D flower-like bimetallic phosphide with a climbing effect on overall water splitting, Applied Catalysis B: Environmental, 279 (2020) 119396.
[59] A. Humayun, N. Manivelan, K. Prabakar, Charge Transfer in n-FeO and p-α-Fe2O3 Nanoparticles for Efficient Hydrogen and Oxygen Evolution Reaction, Nanomaterials, 14 (2024) 1515.
[60] J. Zeng, M. Peng, Y. Dong, M. Huang, W. Jin, L. Lai, C. Li, Q. Wu, W. Shu, Y. Song, J. Zhang, A. Kong, J. Li, H. Zhang, Rational design of multi-component Fe(OH)3/Ni-NiO heterostructures bifunctional catalyst for electrochemical water splitting, Molecular Catalysis, 562 (2024) 114215.
[61] H. Chen, S. Qiao, J. Yang, X. Du, NiMo/NiCo2O4 as synergy catalyst supported on nickel foam for efficient overall water splitting, Molecular Catalysis, 518 (2022) 112086.
[62] X. Yan, L. Tian, S. Atkins, Y. Liu, J. Murowchick, X. Chen, Converting CoMoO4 into CoO/MoOx for Overall Water Splitting by Hydrogenation, ACS Sustainable Chemistry & Engineering, 4 (2016) 3743-3749.